Available online at www.sciencedirect.com
ScienceDirect
Journal of Power Sources 162 (2006) 1104–1114
JOURNAL OF POWER SOURCES
www.elsevier.com/locate/jpowsour

The dynamic behavior of pressure during purge process in the anode of a PEM fuel cell

Jun Gou, Pucheng Pei *, Ying Wang

State Key Laboratory of Automotive Safety and Energy, Tsinghua University, Beijing 100084, China

Received 15 June 2006; received in revised form 20 July 2006; accepted 20 July 2006
Available online 24 August 2006

Abstract

A one-dimensional mathematic computational fluid dynamics model of a proton exchange membrane (PEM) fuel cell is presented in this paper to simulate the transient behavior of hydrogen pressure in the flow field during a typical dynamic process—the purge process. This model accounts for the mechanism of pressure wave transmission in the channels by employing the characteristic line method. A unique parameter—pressure swing, which represents the top value of pressure variation at certain point in the channel during the purge process, is brought up and studied as well as the pressure drop. The pressure distribution along the channel and the pressure drop during the purge process for different operating pressures, lengths of purge time, stoichiometric ratios and current densities are studied. The results indicate that the distributed pressure, pressure drop and pressure swing all increase with the increment of operating pressure. With a high operating pressure a second-falling stage can be seen in the pressure drop profile while with a relatively low operating pressure, a homogeneous distribution of pressure swing can be attained. A long purge time will provide enough time to show the whole part of the pressure drop curve, while only a part of the curve can be attained if a short purge time is adopted, but a relatively uniform distribution of pressure swing will show up at the moment. Compared with the condition of stoichiometric ratio 1, the pressure drop curve decreases more sharply after the top value and the pressure swing displays a more uniform distribution when the ratio is set beyond 1. Different current densities have no apparent influence on the pressure drop and the pressure swing during this transient process. All the distribution rules of related parameters deducted from this study will be helpful for optimizing the purging strategies on vehicles.

Keywords: PEM fuel cell; Purge; Dynamic pressure; Simulation

1. Introduction

PEM fuel cells are considered as one of the most promising alternative power devices for both stationary and mobile applications. However, with regard to the longevity, the fuel cells for vehicle use inevitably cannot survive as a long period as for the stationary application. The reason may lie in the fact that the fuel cells for vehicle use frequently experience dynamic conditions which accelerate the aging process of the fuel cells [1]. Pressure wave transmission generated in the flow channels during the dynamic processes may lead to mechanical vibrations of the membrane electrode assembly (MEA) and accelerate its damaging. [2]. Early dynamic model by Amphlett et al. [3] based on coupling the steady state electrochemical model with an unsteady thermal model predicted the transient electrical response of start-up, load-step and slow-down operating conditions. Most of the following dynamic models [1,4–6] in the past were also set up to simulate the transient behaviors of current–voltage relation polarization curve, or develop modeling methods and experimental techniques for the study of current distribution under transient conditions [7,8], whereas few calculations have concentrated on the dynamics of pressure and flow conditions or specially modeling the transient response of pressure distribution in the flow channels. Though there had been many excellent models through CFD approach to simulate the flow and the along-channel pressure drop [9,10], most of them were limited to the pressure characteristics under steady state. Pathapati et al. [11] proposed a transient mathematical model incorporating the effects of dynamics of flow and pressure in both anode and cathode side and charge double layer to simulate the dynamic response of pressure as well as voltage output. However, the dynamic properties of pressure presented by

* Corresponding author. Tel.: +86 10 62789134; fax: +86 10 62785708.
E-mail address: phcpei@tsinghua.edu.cn (P. Pei).

0378-7753/$ – see front matter © 2006 Elsevier B.V. All rights reserved.
doi:10.1016/j.jpowsour.2006.07.039

them only characterize the average pressure in channels, while the pressure wave at certain point or non-uniformity of pressure distribution could not be caught since uniform pressure in the flow field has been assumed. Um et al. [12] developed a multidimensional model through CFD approach to simulate the transient details of electrochemical kinetic, current distribution, hydrodynamics and multicomponent transport in PEMFC. They studied the non-uniformity in the flow field during transient processes, but as mentioned above, this study also focused on the dynamic behaviors of polarization relation and local current distribution. Although the along-channel distribution of reactant and water vapor fraction had been presented simultaneously, the concentration of this study was still on the basis of performance output, other than the potential damages from the pressure dynamics in channels. Since the membrane electrode assembly (MEA) of fuel cell suffers from frequent pressure fluctuations generating in the channels during dynamic processes, a comprehensive understanding about the phenomena and regularity of pressure distribution is indispensable to improve the controlling strategies for various transient processes. Another important point that should be mentioned is that numerous dynamic simulations have been proposed while experimental data about the dynamic processes are scarce in the present. This work is to pursuit the dynamic characteristic of pressure in the flow field during a typical dynamic process—the purge process based on one-dimensional non-steady fluid simulation and experiments.

2. Model development

The PEM fuel cell model presented here is a one-dimensional, transient, computational model providing a detailed description of the following phenomena during the purge process on different operating conditions:

1. transient distribution of pressure along the channel in the anode;
2. pressure drop of the gas flow in the anode.

The equations governing the purge process include the mass and momentum conversion equation governing fluid flow, procedure equations governing the assumed isentropic process and the ideal gas state equation.

The governing equations and appropriate boundary conditions were implemented and solved in MATLAB environment based on the characteristic line method which has been classified as an excellent solution for the one-dimensional unsteady flow condition solving [13].

2.1. Assumptions

A complete computational fluid dynamics model of the flow field in fuel cell will involve many complex factors and related equations, which make the model complicated. Therefore, some assumptions should be made to simplify the model.

From a typical profile of pressure curve during the purge process shown in Fig. 1, the pressure variation can be divided into three stages: trailing edge, wave hollow and rising edge. According to numerous wave forms collected from the tests, consistent with the curves in Fig. 1, it can be concluded that the rising stage has to take relatively long time to recovery the initial pressure, compared with the other two stages. Since the recovery process proceeds smoothly and no fluctuations of pressure has been observed, the rising stage is ignored in this simulation to save the computational resource and improve the efficiency of calculation.

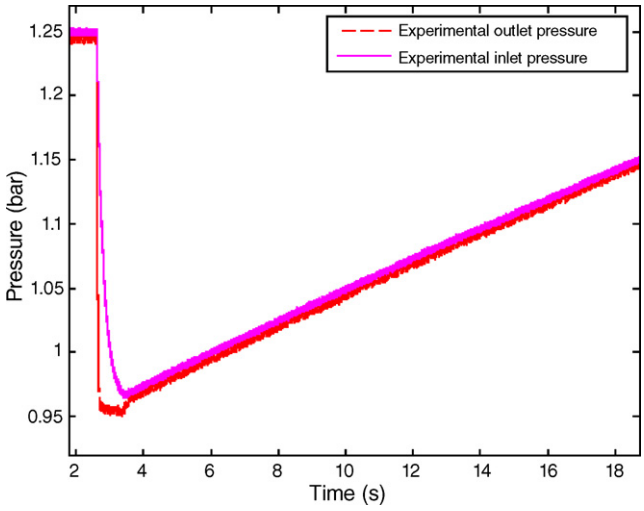

Fig. 1. A typical pressure curve of the purge process.

The modeled period including the trailing edge and the wave hollow lasts a very short time, usually less than 2 s, so the heat transfer between the gas flow and outside during this period can be ignored and an isentropic flow condition is assumed here. Thus, the energy equation can be neglected in the model. The adiabatic index k is assumed to be a constant and k is only related to the diatomic gas H_2.

The effect of the channel bends on the pressure drop is ignored here and the frictional is taken as the total pressure drop in the channel. The discrete pressure drop due to the bends in the channel is much less than the frictional pressure drop due to the viscosity of gas flow, and a calculated frictional pressure drop can be very near to the experimental data [14].

In the channels, water is assumed to exist in the vapor phase. This assumption is made to eliminate the two-phase flow condition in the model. While the liquid water may exist in practice, this is beyond the scope of this work.

Other assumptions used in this model are:

1. The hydrogen gas is assumed to be fully saturated by water vapor and the mixture of hydrogen gas and water vapor behaves as compressible ideal gas in the anode channels.
2. The flow is assumed laminar due to the low characteristic Reynolds number. The entrance and exit effect are neglected due to the length of channel.
3. Similar flow conditions are assumed in all of the channels.

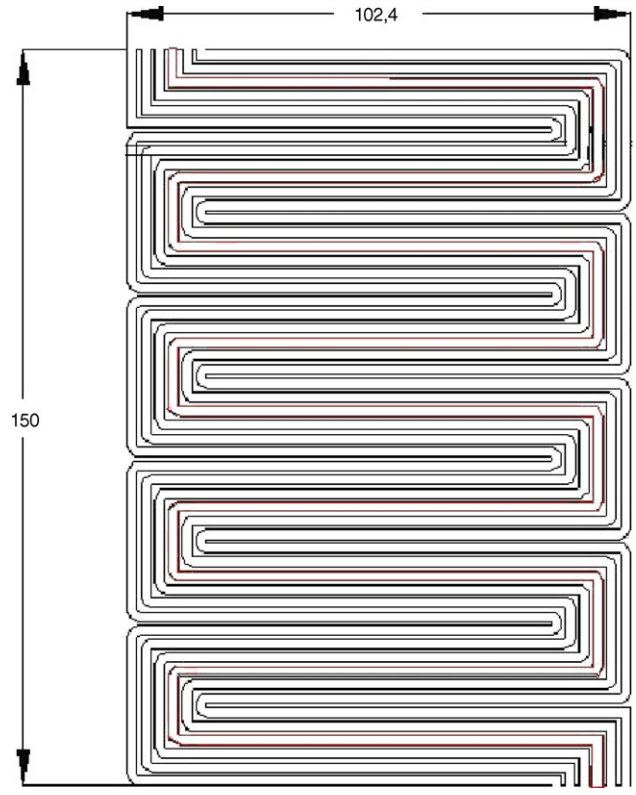

Fig. 2. Geometry of serpentine flow channel fuel cell. The red single channel will be the computational domain. (For interpretation of the references to color in this figure legend, the reader is referred to the web version of the article.)

2.2. Computational domain

A computational model of all the channels in the flow field requires excessively large computing resource, and since the similar flow conditions among all the channels are assumed, the calculation can be based on one serpentine channel shown in Fig. 2, which is shown by the red lines.

The computational mesh named position diagram [13] is shown in Fig. 3. The coordinates in the x–t plane represent the distance from the inlet along the channel and the time, respectively. The steps for calculation are determined differently for the two coordinates: the time step depends on the length of calculated time, or rather the purge time and the accuracy needed for the calculation; while the distance step should be determined by the stability condition of the characteristic line method [13]. Here, the steps chosen for all the calculations are 0.1 s and 0.1545 m and the calculations have all been obtained on a PC with 2.4 GHz Pentium IV.

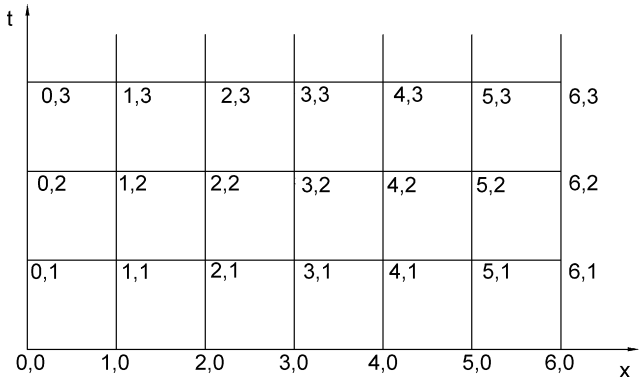

Fig. 3. Rectangular grid on the x–t plane for calculation.

2.3. Governing equations

In the fuel cell channel, the one-dimensional non-steady flow is governed by the continuity equation:

$$\frac{\partial \rho}{\partial t} + \frac{\mathrm{d}(\rho u)}{\mathrm{d}x} = 0 \tag{1}$$

and momentum equation:

$$\frac{\partial u}{\partial t} + u\frac{\partial u}{\partial x} + \frac{1}{\rho}\frac{\partial p}{\partial x} = 0 \tag{2}$$

where ρ, p and u are the density of the gas mixture, gas pressure and flow rate in the channel, respectively.

Since the isentropic flow is assumed in this model, energy equation can be neglected, but the whole process modeling here will be governed by the procedure equation due to this assumption:

$$\frac{p}{\rho^k} = \text{constant} \tag{3}$$

The state of all the gaseous species are governed by the ideal gas state equation:

$$p = \rho RT \tag{4}$$

where R is the universal gas constant and T is the temperature of the gas in the channel.

The equations above make a set of fundamental equations of the model. With the sonic equation: $\alpha = \sqrt{\mathrm{d}p/\mathrm{d}\rho} = \sqrt{k(p/\rho)}$ [13] and Eq. (3): p/ρ^k = constant, Eq. (1) becomes

$$\frac{\partial \alpha}{\partial t} + u\frac{\partial \alpha}{\partial x} + \frac{k-1}{2}\alpha\frac{\partial u}{\partial x} = 0 \tag{6}$$

and Eq. (2) becomes

$$\frac{\partial u}{\partial t} + u\frac{\partial u}{\partial x} + \frac{2\alpha}{k-1}\frac{\partial \alpha}{\partial x} = 0 \tag{7}$$

To invert Eqs. (6) and (7) into ordinary differential equations, two combinations have been made: Eq. (6) $\pm(k-1)/2$ Eq. (7), then the following equations are attained:

$$\left[\frac{\partial \alpha}{\partial t} + (u+\alpha)\frac{\partial \alpha}{\partial x}\right] + \frac{k-1}{2}\left[\frac{\partial u}{\partial t} + (u+\alpha)\frac{\partial u}{\partial x}\right] = 0 \tag{8}$$

$$\left[\frac{\partial \alpha}{\partial t} + (u-\alpha)\frac{\partial \alpha}{\partial x}\right] - \frac{k-1}{2}\left[\frac{\partial u}{\partial t} + (u-\alpha)\frac{\partial u}{\partial x}\right] = 0 \tag{9}$$

Eqs. (8) and (9) are obtained from the set of fundamental governing equations, therefore the solutions of these two equations equal to the ones of the set of fundamental equations.

For Eqs. (8) and (9), if

$$\frac{\mathrm{d}x}{\mathrm{d}t} = u \pm \alpha \tag{10}$$

then Eqs. (8) and (9) become

$$\frac{d\alpha}{dt} \pm \frac{k-1}{2}\frac{du}{dt} = 0 \tag{11}$$

Eqs. (10) and (11) constitute the ordinary differential equations of the model. For the calculation with the characteristic line method, non-dimensional parameters are generally used, as the following defines [13]:

$$A = \frac{\alpha}{\alpha_R} = \left(\frac{p}{p_R}\right)^{(k-1)/2k}, \qquad U = \frac{u}{\alpha_R}, \qquad X = \frac{x}{l_R},$$
$$Z = \frac{\alpha_R t}{l_R} \tag{12}$$

where α_R, p_R and l_R are the reference sonic velocity, the reference pressure and the reference length and A, U, X and Z denote the non-dimensional pressure, the non-dimensional flow rate, the non-dimensional length and the non-dimensional time. Therefore, the ordinary differential equations of the model with non-dimensional parameters become

$$\frac{dX}{dZ} = U \pm A \tag{13}$$

$$\frac{dA}{dZ} \pm \frac{k-1}{2}\frac{dU}{dZ} = 0 \tag{14}$$

2.4. Boundary condition and model parameters

From the items: $A = (\alpha/\alpha_R) = (p/p_R)^{(k-1)/2k}$ and $U = u/\alpha_R$ in Eq. (12), the boundary conditions of this model depend on the pressure and the velocity at the inlet and outlet of the channel.

At the outlet, pressure boundary condition is applied and the impulse of pressure during the purge process is described as the following:

$$\begin{cases} A_{out}^{2k/(k-1)} p_R = A_0^{2k/(k-1)} p_R - b_p t, & 0 \le t \le t_p \\ A_{out}^{2k/(k-1)} = A_R^{2k/(k-1)}, & t > t_p \\ b_p = \dfrac{A_0^{2k/(k-1)} - A_R^{2k/(k-1)}}{t_p} p_R \end{cases} \tag{15}$$

where A_0 and A_R denote the initial and the ending values of the non-dimensional pressure at the outlet, A_{out} stands for the value of the non-dimensional pressure at the outlet and b_p and t_p represent the slope coefficient of pressure decreasing and the time of trailing edge of the purge process, respectively.

At the inlet, a quasi-steady flow condition is assumed here because when the hydrogen gas is inducted from a gas source into the channel, the variations of the parameters change more dramatically on the x-axis than on the t-axis. Therefore, the condition of parameters at the inlet in this transient process can be described by the energy equation of steady flow condition

$$A_s^2 = A_{in}^2 + \frac{k-1}{2}U^2 \tag{16}$$

where A_s and A_{in} denote the values of the non-dimensional pressures in the gas store and at the inlet, respectively. For every case modeled, the non-dimensional pressure in the store is a constant, but the non-dimensional pressure and non-dimensional flow rate at the inlet will change dramatically with the pressure impulse at the outlet during the purge process.

The initial value of $A(Z=0)$ is determined by the equations: $A_s = (p_s/p_R)^{(k-1)/2k}$, $A_{in} = (p_{in}/p_R)^{(k-1)/2k}$, $A_{out} = (p_{out}/p_R)^{(k-1)/2k}$ and $p_{out} = p_{in} - \Delta p$. Here, p_s denotes the pressure in the gas store and the initial value of p_s varies with different cases: 1.50, 1.75 and 2.00 bar and Δp is the pressure drop of the whole channel in steady state, which can be calculated exactly based on the equation provided in ref. [14]. In this work, the initial values of pressure drop of the purge process were obtained from the corresponding tests in steady state. As assumed above, the frictional pressure drop is taken as the total pressure drop, thus the initial values of pressure at other calculated positions along the channel can be obtained with the liner interpolation method.

The initial value of hydrogen gas consumption is given by

$$H_2 \text{ usage} = \frac{I}{2 \times F} = 5.182 \times 10^{-6} \times I \tag{17}$$

where F and I denote the Faraday constant and the current of the fuel cell.

Since the saturated hydrogen gas is assumed in the channel, the molar fraction of water vapor is given by ref. [15]

$$x_w = \frac{p_w^{sat}}{p} \tag{18}$$

where the subscript "w" denotes the water vapor and "sat" means saturation value. p_w^{sat} depends on the inlet gas temperature T_{in}. According to the ideal gas state equation: $V = (nRT)/p$, the volume flux of the humidified hydrogen gas can be given by

$$Q_{in} = \frac{H_2 \text{ usage} \times RT_{in}}{p(1 - x_w)} = \frac{5.182 \times 10^{-6} IRT_{in}}{p(1 - x_w)} \tag{20}$$

where the subscript "in" denotes the parameters at the inlet.

Therefore, the initial value of non-dimensional flow rate $U(Z=0)$ can be given by

$$U = \frac{u}{\alpha_R} = \frac{Q_{in}}{dh\sqrt{kRT_R}} \tag{21}$$

where T_R stands for the reference temperature and d and h represent the geometric width and depth of the channel.

The parameters used for the base case simulations presented here are shown in Table 1.

2.5. Supplemental conditions in algorithm

The ordinary differential equations and appropriate boundary conditions above can be solved based on the algorithm of the characteristic line method to obtain the distribution of pressure in the channel. However, in this work, the compensating effects of two regulators—the relieve valve unit and the flux controller on the transients of pressure and velocity must be considered in the calculation.

The relieve valve unit sets the value of induction pressure and regulates the pressure when there are some fluctuations of

Table 1
Geometrical, operational parameters for the cases

Property	Value
Channel length, L (m)	0.927
Channel width, d (m)	0.002
Channel height, h (m)	0.0008
Area of the active area of the MEA, S (m^2)	154×10^{-4}
The initial value of temperature, T (K)	323
Inlet gas temperature, T_{in} (K)	323
Pressure in the gas store, p_s (bar)	1.50, 1.75 and 2.00
The initial value of pressure drop, Δp (bar)	0.004 and −0.012
Reference length, l_R (m)	0.927
Reference temperature, T_R (K)	298
Reference pressure, p_R (bar)	1.01
Current, I (A)	92.4, 123.2 and 154
Hydrogen stoichiometric ration, λ_a	1, 1.1, 1.2
Adiabatic index, k	1.4
The universal gas constant, R (kJ mol^{-1} K^{-1})	8.314
Trailing edge time of the purge process, t_p (s)	0.07–0.15

the pressure behind the valve. The flux meter works as a flux controller when the real flux of gas flow exceeds the value set previously and otherwise it is used just as a flux meter. Therefore, when the pressure suddenly decreases and the flux exceeds the value set beforehand during the purge process, the relieve valve unit and the flux meter will regulate the parameters as feedback controllers. Since the technical data with the relieve valve unit and the flux meter cannot exactly describe their compensating effects in this transient process, two iterative equations are introduced in the calculation to simulate the contributions of these two regulators in this transient process.

$$p_{r+1} = p'_{r+1} + (p_r - p'_{r+1}) \times c_1;$$
$$u_{r+1} = u'_{r+1} + (u_r - u'_{r+1}) \times c_2. \quad (22)$$

where p_{r+1} and u_{r+1} are the pressure and the flow rate value coupling the compensating effects of the regulators, while p'_{r+1} and u'_{r+1} are the ones without coupling these compensating effects, the subscript "r + 1" stands for the sequence of the time step and c_1, c_2 are the compensating factors dependent on the regulators themselves. With Eq. (12), the two iterative equations become

$$A_{r+1}^{2k/(k-1)} = A'^{2k/(k-1)}_{r+1} + \left(A_r^{2k/(k-1)} - A'^{2k/(k-1)}_{r+1}\right) \times c_1;$$
$$U_{r+1} = U'_{r+1} + (U_r - U'_{r+1}) \times c_2. \quad (23)$$

These equations supplement the compensating effects of the two regulators on the transient behaviors of pressure and flow rate in the calculation, which improve the accuracy of the modeling. To simulate the characteristics of these two regulators accurately, numerous tests on different operating conditions are necessary to decide the corresponding factors before the calculation.

3. Results and discussions

3.1. Experimental validation

To validate the numerical model presented above, three comparisons with different operating pressures, lengths of purge time and current densities were made between simulation results and experimental data. The experiments were conducted on a test bench shown in Fig. 4.

As Fig. 4 shows, the pressure and flux of inlet hydrogen gas were controlled and stabilized by relieve valve unit and flux controller, respectively. The temperature and pressure of inlet and outlet gas were both recorded by the collector with 50 kHz frequency. In the terminal of the flow pipe, two outlet valves were set and the transient purge process can be realized using electromagnetic valve.

The pressure measurements for the purge process were made under the condition of 50 °C cell temperature. The hand operated valve was closed before the purge process, thus the anode stoichiometric ratio was 1. This condition was chosen close to the

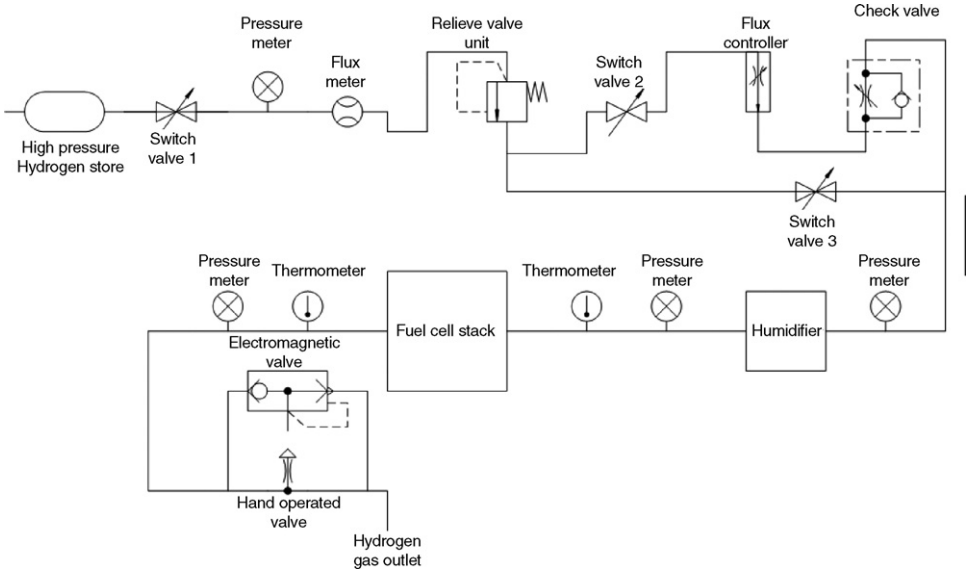

Fig. 4. PEM fuel cell testing bench.

one under which water accumulations in the channels easily took place, followed by purge processes in the real operating conditions. The reactants were fully humidified by setting a higher dew point temperature than that of the cells. It should be noted that *significant* water accumulations in the flow field must be avoided in the tests in which two-phase flow should be considered. As the assumption mentions above, that condition has been out of the scale of this study.

The outlet pressure profiles were attained through the tests and then adapted as the input conditions of the simulations, accordingly the inlet pressures can be obtained from both simulations and tests. Figs. 5–7 show the comparisons between the simulation results and the experimental data at three different operating pressures, lengths of purge time and current densities, respectively. Good agreements can be seen in the comparative profiles of inlet pressure. Inadequate agreement for the comparative profiles of outlet pressure is attributed to the fact that all the outlet pressure profiles were simplified into liner trailing edge in simulation, while the real pressure at the outlet might fluctuate with the pressure in pipes slightly. But the trend can be still captured by the present model. Pressure non-uniformity during this transient process can be displayed by these simulation results that are unattainable from experiments.

3.2. Pressure distribution during the purge process

A detailed distribution of local pressure in the channel is shown in Fig. 8. As expected, a nearly uniform decreasing trend of distributed pressure would result when a low operating pressure like 1.25 bar is adopted, except that some short stable periods of pressure take place at the points ($X/L = 1/2$, 2/3 and 5/6) in the channel immediately after the trailing edge. These may be caused by the relatively short trailing edge in this experiment, thus they are the reflections of pressure wave superposition which actually slow up the decreasing process. Obviously, it can also be indicated from the figure that the points in the downstream or close to the exit of channel will be influenced by the trailing edge of pressure more noticeably and the stable pressure can be attained more quickly than the ones far from the channel exit. Here, one unique parameter—pressure swing is defined as the highest amplitude of pressure variation at certain point during the whole process modeled, and actually it represents the mechanical attack of gas flow to the membrane electrode assembly in this transient processes. The pressure swing versus fractional location along the channel flow path is given in Fig. 9. From Fig. 9, a nearly homogeneous pressure swing distribution can be seen. This is due to the fact that both the local highest and the lowest pressure, actually the initial and the stable value, along the flow path decrease slightly during the process when a relatively low operating pressure is adopted.

3.3. Pressure difference effects

Pressure distribution during the purge process is influenced greatly by the operating pressure since the ending pressures of the processes for all the experiments and simulations are set close to the standard atmosphere pressure. Fig. 10 shows the plots of

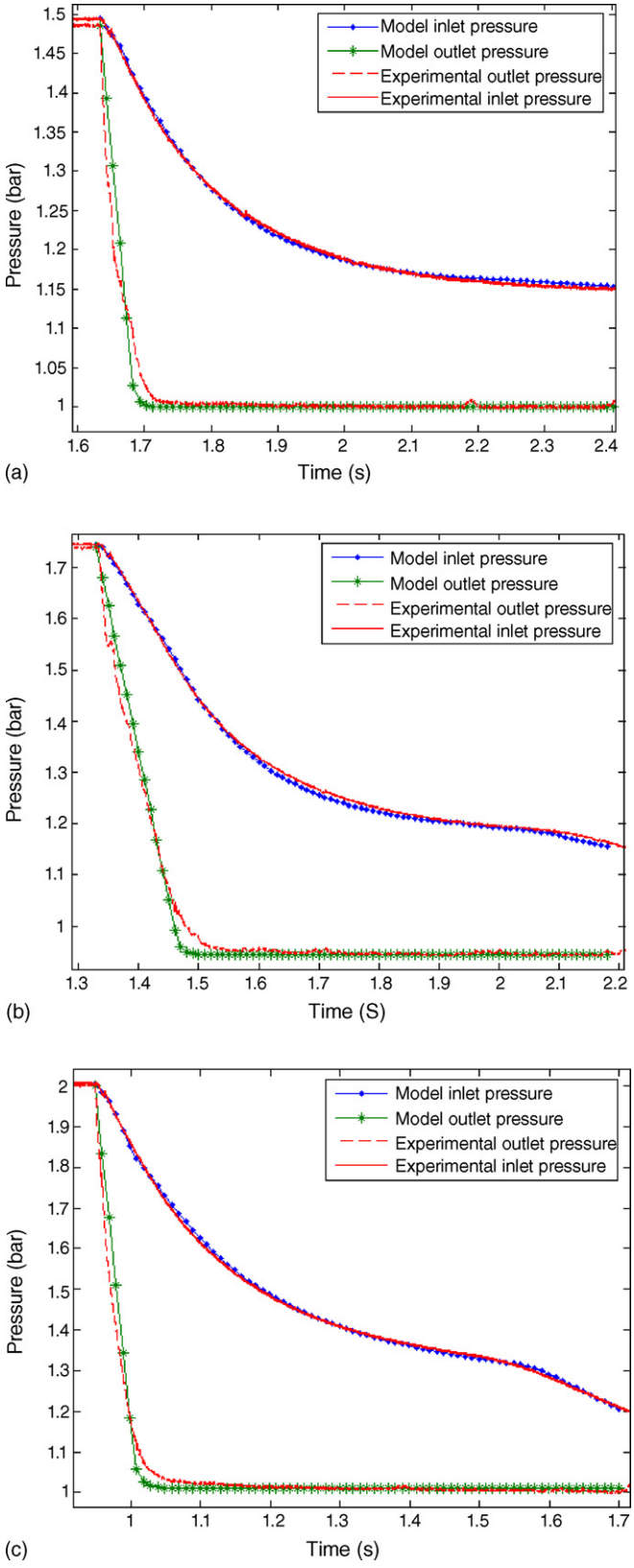

Fig. 5. Comparison of experimental and model pressure curves during the purge process for three different operating pressures: (a) 1.50 bar, (b) 1.75 bar and (c) 2.00 bar. $\lambda_a = 1$ at 1.0 A cm^{-2}; purge time, 0.7 s; operating pressure, 2.00 bar.

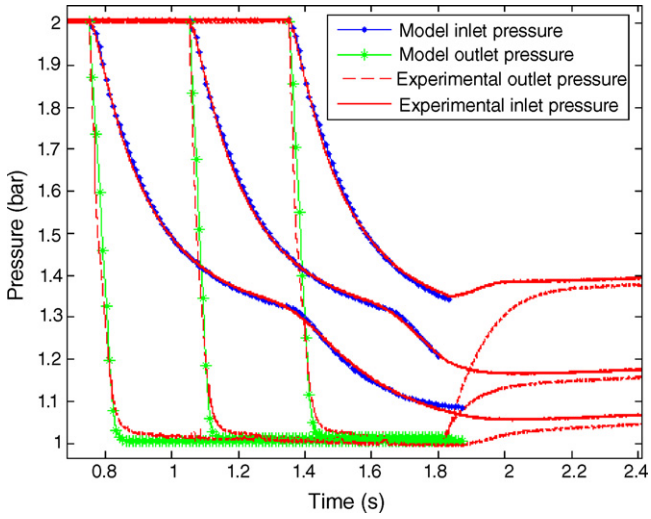

Fig. 6. Comparison of experimental and model pressure curves during the purge process for three different lengths of purge time: 1.0, 0.68 and 0.36 s (from left to right). $\lambda_a = 1$ at 1.0 A cm^{-2}; operating pressure, 2.00 bar.

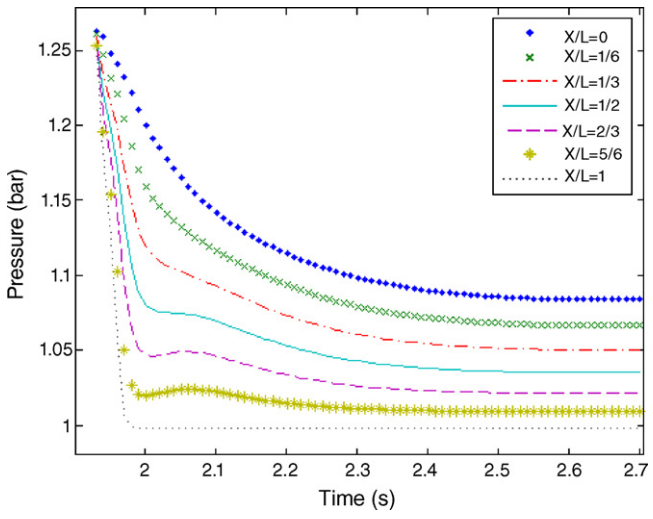

Fig. 8. Pressure distributed curves during the purge process for a low operating pressure 1.25 bar. $\lambda_a = 1$ at 1.0 A cm^{-2}; purge time, 0.7 s.

pressure behaviors at different positions in the flow field during the purge process for three different operating pressures. With the increment of operating pressure from 1.50 to 2.00 bar, all the distributed pressure curves are enhanced to new levels by steps except the outlet pressure profile, which means that the pressure value at the same instant for every preset point will be improved due to the increased operating pressure. As can be seen from the figures, when the operating pressure exceeds 1.75 bar, in Fig. 10b and c, a second-falling pressure profile endings are added to the curves. The pressure variations at the points near the inlet of flow field experience another decrease process after the apparently stable period of pressure with a much slower decreasing rate, however this kind of decrease in the end of the purge process cannot be observed while the operating pressure is relatively low, at 1.50 bar. The apparently stable stage of pressure decreasing is probably due to a high pressure ratio between inlet and outlet, which leads to more pressure wave superposition with high values and consequently slows the decreasing process. With the weakening of the pressure wave amplitude, the second-falling stage shows up. During the terminal stage of the purge process, or rather close to the ending, the pressure drop between every two preset positions decreases along the channel for the relatively low operating pressure (1.50 bar), but the trend changes since the second-falling stages show up for the relatively high operating pressures. In Fig. 10b, the pressure drops between two adjacent points upstream in the end of process is mostly equal to those downstream. When the operating pressure rises up to 2.00 bar in Fig. 10c, the pressure drops between two adjacent points upstream are much higher than those downstream. As a conclusion, in the ending of the purge process, the whole pressure drop will be contributed more by the downstream field of the channel with the operating pressure increasing, other than equally contributed by every area in the flow field.

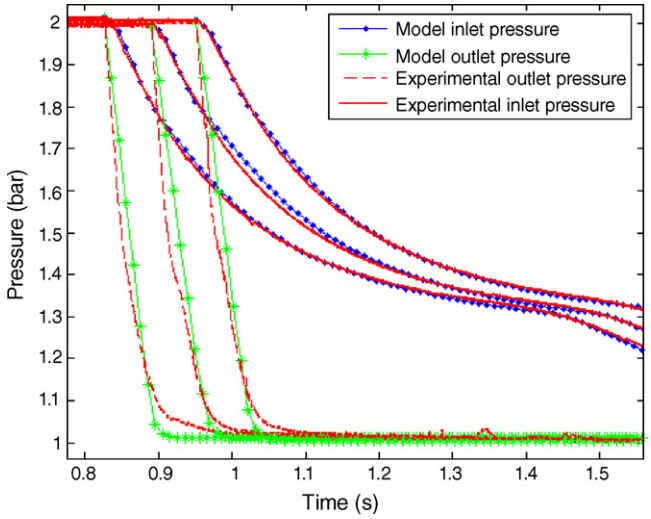

Fig. 7. Comparison of experimental and model pressure curves during the purge process for three different current densities: $J = 0.6$, 0.8 and 1.0 A cm^{-2} (from left to right). $\lambda_a = 1$; purge time, 0.64 s; operating pressure, 2.00 bar.

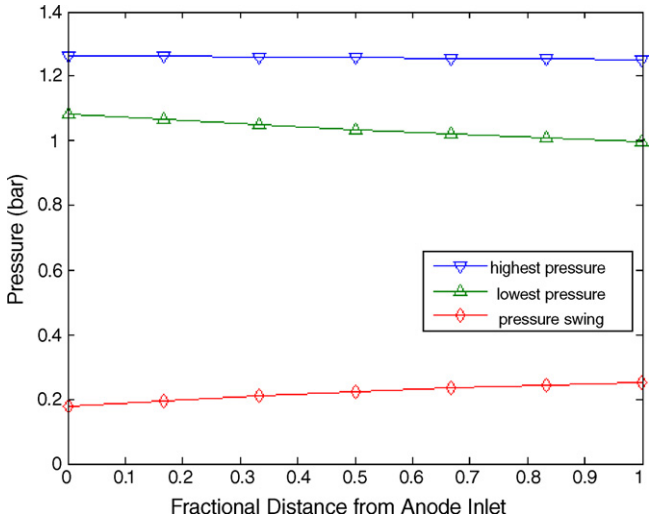

Fig. 9. Pressure swing vs. fractional location along the anode channel during the purge process for a low operating pressure 1.25 bar. $\lambda_a = 1$ at 1.0 A cm^{-2}; purge time, 0.7 s.

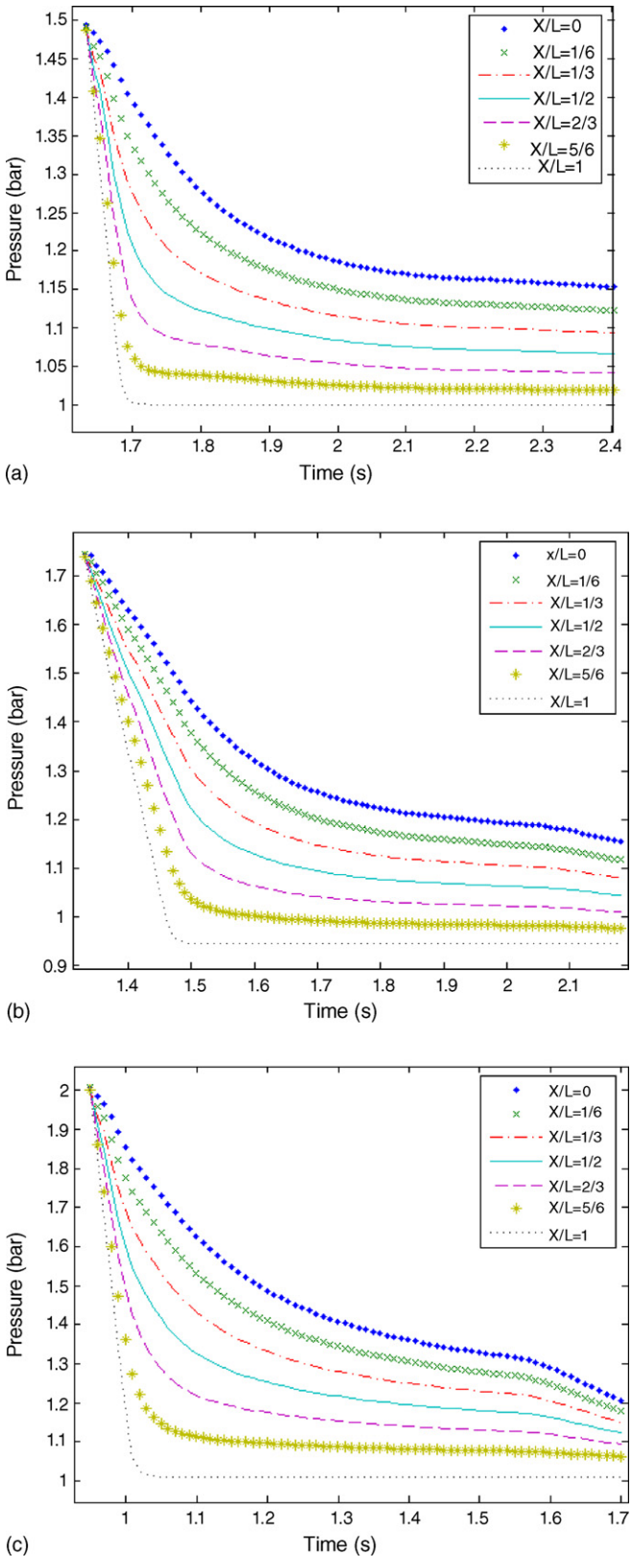

Fig. 10. Pressure distributed curves during the purge process for three different operating pressures: (a) 1.50 bar, (b) 1.75 bar and (c) 2.00 bar. $\lambda_a = 1$ at 1.0 A cm^{-2}; purge time, 0.7 s.

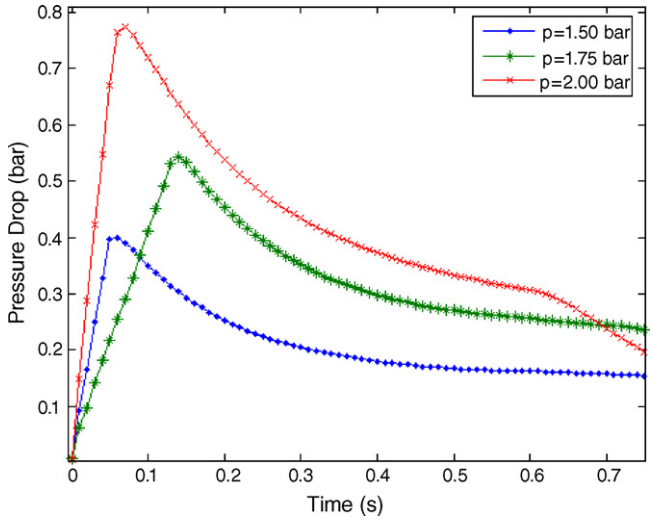

Fig. 11. Pressure drop curves during the purge process for three different operating pressures: 1.50, 1.75 and 2.00 bar. $\lambda_a = 1$ at 1.0 A cm^{-2}; purge time, 0.7 s.

Fig. 11 gives the comparison of pressure drop curves for three different operating pressures. It can be seen that the top and the average value of pressure drop during the purge process increases with the operating pressure. Since there will be the second-falling decreasing stage for relatively high operating pressure, like at 2.00 bar, the purge time can be chosen appropriately based on the rules, which is probably deducted from Fig. 11, to improve the purging efficiency by prolonging the periods with high pressure drop before the second-falling decreasing stage comes.

Fig. 12 shows the pressure swing distribution along the channel during the process. Similarly with the pressure drop variation, the pressure swing value at every calculated point increases with the operating pressure. The distribution of pressure swing at a lower operating pressure seems a little homogeneous than the one at a higher operating pressure. However, the uniform trend of pressure swing variation for all the cases is that the value

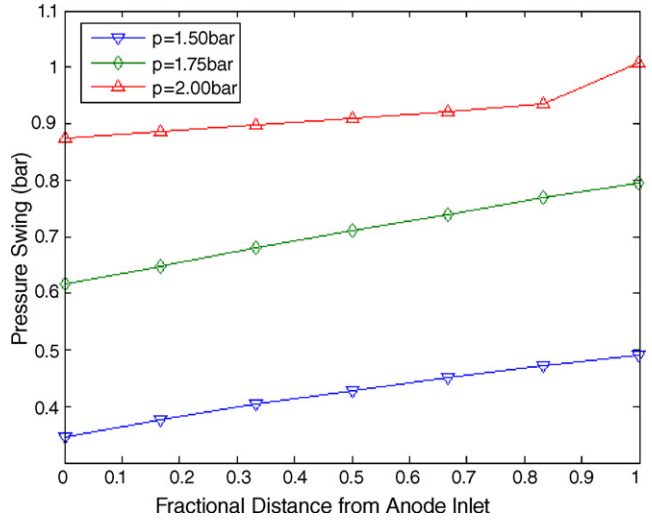

Fig. 12. Pressure swing vs. fractional location along the anode channel during the purge process for three different operating pressures: 1.50, 1.75 and 2.00 bar. $\lambda_a = 1$ at 1.0 A cm^{-2}; purge time, 0.7 s.

increases along the channel, which is even more pronounced at higher operating pressures. Pressure swing, as explained above, reflects the highest impulse of pressure at certain point and mechanical effects on the membrane electrode assembly. Therefore, the area of the MEA close to the exit of flow field always suffers the top mechanical attacks of gas flow in this transient process, although this effect seems uniform in some degree in the channel at low operating pressure.

3.4. Purge time effects

The length of purge time is a key factor to be considered when the purging strategy is made. Experiments and the corresponding simulations with the same operating pressure 2.00 bar, and current density 1 A cm^{-2}, but with different lengths of purge time: 0.36, 0.68 and 1.0 s, were conducted to test the effect of the length of purge time on pressure drop and pressure swing. In Fig. 13, it can be seen that the profile of pressure drop curve is completely shaped by the length of purge time. The whole profile of the pressure drop, including the stable and the second-falling periods, can be observed if a relatively long purge time (1.0 s) has been chosen, while if a short purge time (0.36 s) is adopted, only a part of the whole profile without the second-falling period can be available. Fig. 14 displays the comparison of the pressure swings for these three cases. As can be seen from the figure, for the short period there is an obvious monotonic increment of pressure swing along the channel. Although the distribution of pressure swing in the whole flow field is non-uniform, the area upstream of MEA receives a low pressure swing, or mechanical effect of the gas flow. Oppositely, for the long purge time the distribution of pressure swing seems more uniform, compared with the one for a short purge time, however the area upstream of MEA may also suffer a higher pressure swing which means more severe attacks of gas flow to the MEA.

As indicated above, a too short purge period will lead to the non-uniformity of distribution of pressure swing or mechanical

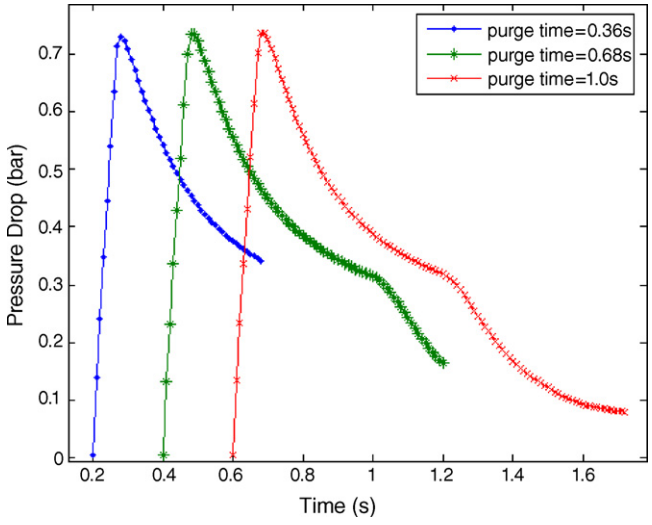

Fig. 13. Pressure drop curves during the purge process for three different lengths of purge time: 0.36, 0.68 and 1.0 s. $\lambda_a = 1$ at 1.0 A cm^{-2}; operating pressure, 2.00 bar.

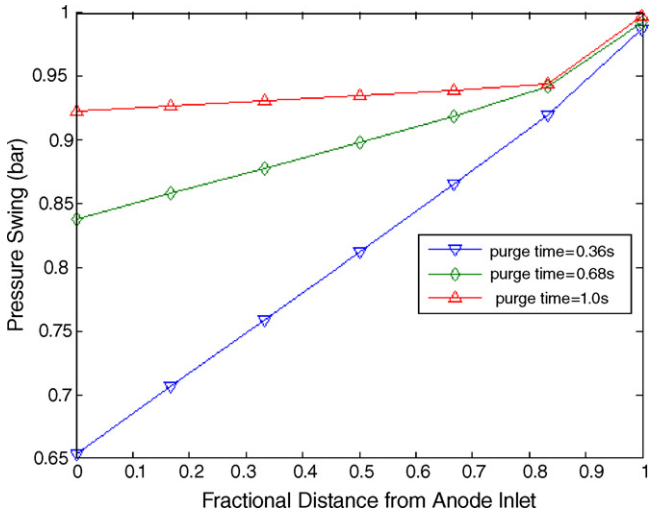

Fig. 14. Pressure swing vs. fractional location along the anode channel during the purge process for three different lengths of purge time: 0.36, 0.68 and 1.0 s. $\lambda_a = 1$ at 1.0 A cm^{-2}; operating pressure, 2.00 bar.

impulse of gas flow on MEA, and the high pressure drop period cannot be made full use of to gain an efficient purge process, while a too long purge time may include some periods with low pressure drop that would be useless for a better purge process, and the area upstream of MEA has to suffer high pressure swings and severe attacks of gas flow, which may damage the MEA if they take place frequently. Therefore, the length of purge time should be chosen appropriately for an efficient purge process with low potential damaging to the components.

3.5. Hydrogen stoichiometric ratio effects

All the simulations and experiments discussed above were conducted in condition that the hydrogen outlet was closed down and the purge processes were accomplished by the electromagnetic valve, thus the hydrogen stoichiometric ratio $\lambda_a = 1$. Actually in the application of fuel cell, the hydrogen stoichiometric ratio is not always 1 when the hydrogen gas circulation is adopted. The following discussion displays the comparison of the purge processes with different hydrogen stoichiometric ratios.

Experiments with the same operating pressure 2.00 bar and current density 0.6 A cm^{-2}, but with different outlet boundary conditions and hydrogen stoichiometric ratios (1, 1.1 and 1.2), were conducted to test the effect of stoichiometric ratio on the pressure drop and the pressure swing in the purge processes. It can be expected that when the stoichiometric ratio is reset, the whole profile of the pressure variation during the purge process may be modified because the hydrogen gas circulation is added and the outlet boundary condition has changed. Therefore, the validations should be conducted specially, which are shown in Fig. 15. There can also be good agreements between experiments and simulations after some model modifications.

In Fig. 15, it can be seen that when the hydrogen circulation is added and hydrogen stoichiometric ratio is enhanced from 1 to 1.1 or 1.2, the second-falling periods have disappeared and

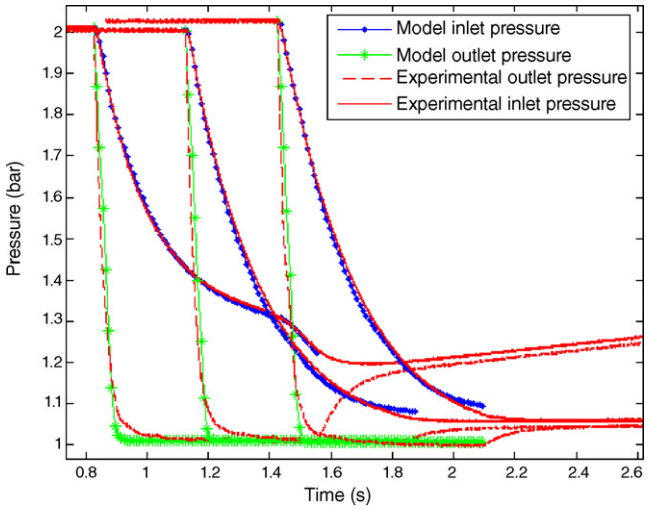

Fig. 15. Comparison of experimental and model pressure curves during the purge process for three different stoichiometric ratios: $\lambda_a = 1$, 1.1 and 1.2 (from left to right). Current density, 0.6 A cm^{-2}; purge time, 0.63 s; operating pressure, 2.00 bar.

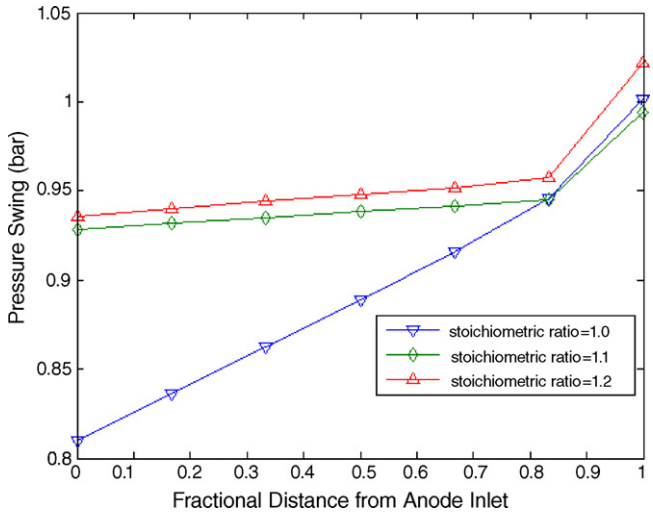

Fig. 17. Pressure swing vs. fractional location along the anode channel during the purge process for three different stoichiometric ratios: $\lambda_a = 1$, 1.1 and 1.2. Current density, 0.6 A cm^{-2}; purge time, 0.63 s; operating pressure, 2.00 bar.

the pressures decrease more dramatically during the purge process. Fig. 16 shows the comparison of pressure drop for the three cases. From this figure, it can be seen that when the stoichiometric ratio is set beyond 1, the pressure drop curves display the sharp decreases after the top pressure drop value other than the period with a high value of pressure drop before the second-falling stage as the situation of the ratio is set 1. In Fig. 17, the pressure swing curves for these cases are given. When the stoichiometric ratio is 1, there is a monotonic increment of the pressure swing along the flow channel, thus the area upstream of MEA may receive a relatively low mechanical effect of gas flow. Oppositely, the distribution of pressure swing in the flow field become more uniform when the stoichiometric ratio is enhanced to 1.1 or 1.2, but in these situations the area upstream of the MEA has to suffer relatively high pressure swing and severe mechanical effect of gas flow.

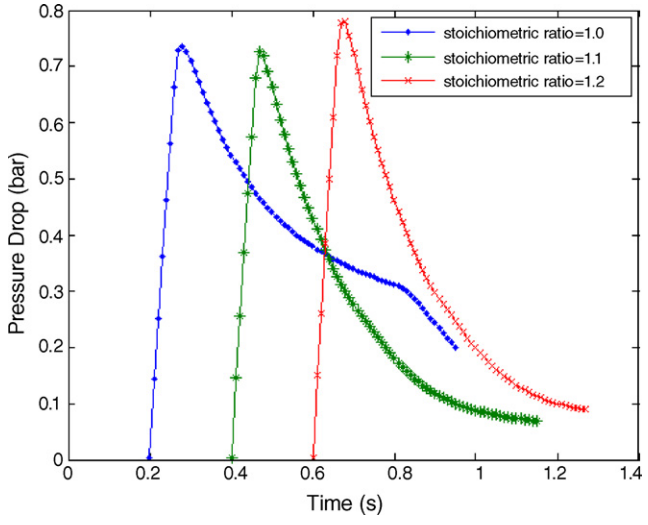

Fig. 16. Pressure drop curves during the purge process for three different stoichiometric ratios: $\lambda_a = 1$, 1.1 and 1.2. Current density, 0.6 A cm^{-2}; purge time, 0.63 s; operating pressure, 2.00 bar.

Therefore, for the purge process, enhancement of the stoichiometric ratio inevitably removes the period with high pressure drop before the second-falling stage that can be used to improve the purging efficiency. Although higher stoichiometric ratios can lead to more uniform distributions of the pressure swing and the mechanical effects of gas flow on the whole MEA, it does improve the potential mechanical attacks of gas flow to the area upstream of MEA, compared with the distribution with stoichiometric ratio 1.

3.6. Current density effects

For the fuel cells on vehicles, different current densities are always required due to various loading requirements, thus the purge process may be conducted under varied power outputs. Current density reflects the consumption of hydrogen gas, which can affect the pressure in the flow field. The following simulations, with the same operating pressure 2.00 bar, stoichiometric ratio 1 and purge time 0.64 s, but with different current densities: $J = 0.6$, 0.8 and 1.0 A cm^{-2} were conducted to test the effect of current density on pressure drop and pressure swing during the purge process.

Fig. 18 displays the pressure drop curves under different current densities. In the comparison, it can be indicated that the operating parameter—current density, has no apparent effect on the pressure variation during this transient process, especially after the top pressure drop value and the curves almost match together. This is probably because the purge process is accomplished in a very short period, during which the gas consumption is too low to show an obvious effect on the pressure in the channel, compared with the compensation of high pressure reactant from the gas source. In Fig. 19, the comparison of pressure swing for the three cases is given. It can be seen that three curves have similar trends—the pressure swing increases

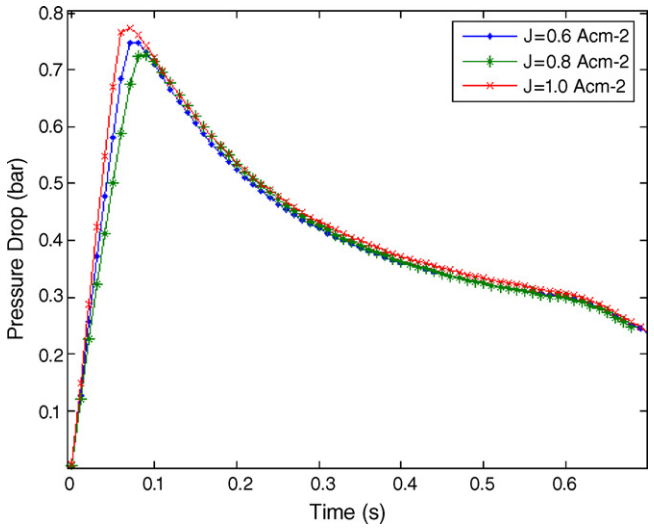

Fig. 18. Pressure drop curves during the purge process for three different current densities: $J = 0.6$, 0.8 and 1.0 A cm^{-2}. $\lambda_a = 1$; purge time, 0.64 s; operating pressure, 2.00 bar.

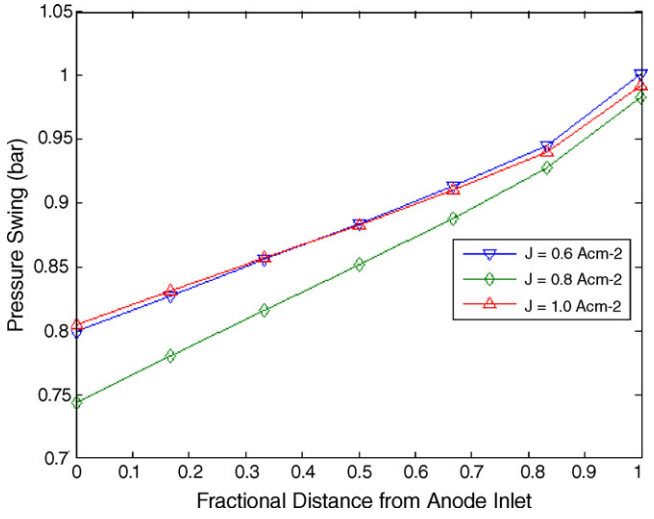

Fig. 19. Pressure swing vs. fractional location along the anode channel during the purge process for three different current densities: $J = 0.6$, 0.8 and 1.0 A cm^{-2}. $\lambda_a = 1$; purge time, 0.64 s; operating pressure, 2.00 bar.

monotonically along the channel. The curve under the current density of $J = 0.8$ A cm^{-2} is slightly lower than others just due to the slightly lower initial operating pressure, which lowers the whole pressure swing curve in some degree.

As indicted above, the current density does not affect the pressure variation obviously during purge processes. Therefore, for vehicle use purging under different loading conditions makes no difference in terms of improving purging efficiency and alleviating the mechanical effects of gas flow or potential damages to the MEA.

4. Conclusions

A one-dimensional computational fluid dynamics model of a PEM fuel cell was developed. The transient behavior of pressure in the channels during purge processes has been studied. The results indicated that the distributed pressure, pressure drop and pressure swing all increased with the increment of operating pressure. With a high operating pressure, the pressure drop profile showed a second-falling stage that can be made full use of to improve purging efficiency, but the pressure swing displayed a homogeneous distribution with a relatively low operating pressure. A long purge time allowed for the whole part of the pressure drop profile, while a short purge time only gave a part of the profile and a relatively non-uniform distribution of pressure swing. When the stoichiometric ratio exceeded 1, the pressure drop curve changed and decreased more sharply after the top value, but the pressure swing displayed a more uniform distribution. Current density did not affect the pressure drop and the pressure swing obviously during this transient process. All the distribution rules of related parameters deducted from this study will be helpful for optimizing the purging strategies on vehicles.

Acknowledgement

Financial supported by the Native High Technique Development Plan (“863”) program fund from Ministry of Science and Technology of China is gratefully acknowledged.

References

[1] A.A. Kulikovsky, H. Scharmann, K. Wippermann, Electrochem. Commun. (6) (2004) 75–82.
[2] R. Jiang, D. Chu, J. Power Sources 92 (1–2) (2001) 193–198.
[3] J.C. Amphlett, R.F. Mann, B.A. Peppley, P.R. Roberge, A. Rodrigues, J. Power Sources 61 (1–2) (1996) 183–188.
[4] S. Kim, S. Shimpalee, J.W. Van Zee, J. Power Sources 135 (1–2) (2004) 110–121.
[5] S. Yerramalla, A. Davari, A. Feliachi, T. Biswas, J. Power Sources 124 (1) (2003) 104–113.
[6] Y. Wang, C.Y. Wang, Electrochim. Acta 50 (6) (2005) 1307–1315.
[7] M.M. Mench, C.Y. Wang, M. Ishikava, J. Electrochem. Soc. 150 (8) (2003) A1052–A1059.
[8] J. Stumper, S.A. Campbell, D.P. Wilkinson, M.C. Johnson, M. Davis, Electrochim. Acta 43 (24) (1998) 3773–3783.
[9] P.T. Nguyen, T. Berning, N. Djilali, J. Power Sources 130 (2004) 149–157.
[10] S. Maharudrayya, S. Jayanti, A.P. Deshpanda, J. Power Sources 138 (2004) 1–13.
[11] P.R. Pathapati, X. Xue, J. Tang, Renew. Energy 30 (2005) 1–22.
[12] S. Um, C.Y. Wang, K.S. Chen, J. Electrochem. Soc. 147 (12) (2000) 4485–4493.
[13] D.M. Jiang, Gas Flow in Internal Combustion Engine, China Machine Press, Beijing, 1986.
[14] P.C. Pei, M.G. Ouyang, W. Feng, L.G. Lu, H.Y. Huang, J.H. Zhang, Int. J. Hydrogen Energy 31 (2006) 371–377.
[15] T. Berning, D.M. Lu, N. Djilali, J. Power Sources 106 (2002) 284–294.